Influence of Structural and Surface Characteristics of $Ti_{1-x}Zr_xO_2$ Nanoparticles on the Photocatalytic Degradation of Methylcyclohexane in the Gas Phase

María D. Hernández-Alonso,*,† Juan M. Coronado,‡ Belén Bachiller-Baeza,† Marcos Fernández-García,† and Javier Soria†

Instituto de Catálisis y Petroleoquímica, CSIC, c/ Marie Curie 2, Cantoblanco, 28049 Madrid, Spain, and Environmental Applications of Solar Radiation, CIEMAT, Avenida Complutense 22, Building 42, Madrid, Spain

Received January 23, 2007. Revised Manuscript Received April 27, 2007

In the present work, we investigate the influence of the physicochemical characteristics of $Ti_{1-x}Zr_xO_2$ nanoparticles with anatase structure on the photocatalytic activity for the elimination of methylcyclohexane in the gas phase. Samples with a molar content of Zr ranging from 0 to 16% were prepared by an inverse microemulsion method. Additionally, a sample of ZrO_2 supported on TiO_2 (5.2% molar content of Zr) was obtained in a two-stage synthesis using the same microemulsion procedure. The structural and electronic properties of these materials were determined by a multitechnique approach using X-ray diffraction as well as Raman, XANES, EXAFS, and UV−vis spectroscopies. FTIR spectra of the catalysts before and after photocatalytic experiments were also carried out in order to evaluate the possible changes on the surface upon photoreaction. In addition, surface characteristics of these nanoparticles were determined by means of N_2 adsorption isotherms and NH_3 adsorption microcalorimetry. XRD and XAS results indicate that the anatase-type structure is maintained throughout the Ti−Zr series, although noticeable changes in the local order are detected for samples above/below 6 % zirconium. All $Ti_{1-x}Zr_xO_2$ samples show a significant enhancement of the photocatalytic activity with respect to both TiO_2 and the ZrO_2/TiO_2 sample at high relative humidity. In contrast, Ti−Zr catalysts exhibit higher deactivation under dry conditions than pure titania. These observations are discussed in relation to the structural and electronic modifications of the anatase nanoparticles induced by Zr incorporation.

1. Introduction

Heterogeneous photocatalytic oxidation is a very promising technology for the removal of volatile organic compounds (VOC's) present in indoor air. Currently, several companies offer air-conditioning systems that incorporate this technology.[1] Those equipments contain a TiO_2 photocatalyst, which is constituted either by the anatase polymorph of this oxide or by anatase−rutile mixtures. This material is used because it is inexpensive, harmless, chemically stable, and it displays a relatively high quantum yield for the elimination of a large number of pollutants.[2,3] Nevertheless, the application of photocatalysis to the purification of severely polluted atmospheres, as those found in some workshops or industrial premises, requires more efficient photocatalysts in order to achieve not only high degradation rates but also to avoid the building-up of partially oxidized compounds. Generation of byproducts can be a serious concern, because some of these molecules can be very noxious (i.e., $COCl_2$).[4] Furthermore, a higher resistance to deactivation and a better performance under solar illumination are also characteristics actively sought in advanced photocatalytic materials.[5,6] All these aspects of the photoactivity are closely connected to the surface and structural characteristics of the catalysts, as several studies have revealed,[7] but further investigation is necessary to gain a complete understanding of these correlations.

To obtain improved photocatalysts, researchers have adopted several strategies. The incorporation of transition metals into the anatase phase of TiO_2 has been frequently studied as a way to extend the spectral response to the visible range.[8] In addition, certain $Ti_{1-x}M_xO_2$ phases show an enhancement of the photoactivity due to structural and electronic modifications induced by the dopant. In this respect, the inclusion of Sn^{4+} in the rutile and the anatase structures leads to a significant increment of the rate for the photocatalytic oxidation of acetone[9] or methylcyclohexane

* Corresponding author. E-mail: mdhernandez@icp.csic.es. Tel: 34915854775. Fax: 34915854760.
† Instituto de Catálisis y Petroleoquímica, CSIC.
‡ Environmental Applications of Solar Radiation, CIEMAT.

(1) Mills, A.; Lee, S-K. *J. Photochem. Photobiol., A* **2002**, *152*, 233−247.
(2) Hoffmann, M. R.; Martin, S. T.; Choi, W.; Bahnemann, D. W. *Chem. Rev.* **1995**, *95*, 69−96.
(3) Linsebigler, A.; Lu, G.; Yates, J. T., Jr. *Chem. Rev.* **1995**, *95*, 735−758.
(4) Ozaki, S.; Zhao, L.; Amemiya, T.; Itoh, K.; Murabayashi, M. *Appl. Catal.* **2004**, *52* (2), 81−89.
(5) Asahi, R.; Morikawa, T.; Ohwaki, T.; Aoki, K.; Taga, Y. *Science* **2001**, *293*, 269−271.
(6) Belver, C.; Lopez-Muñoz, M. J.; Coronado, J. M.; Soria, J. *Appl. Catal., B* **2003**, *46* (3), 497−509.
(7) Yeung, K. L.; Yau, S. T.; Maira, A. J.; Coronado, J. M.; Soria, J.; Yue, P. L. *J. Catal.* **2003**, *219*, 107−116.
(8) Fuerte, A.; Hernández-Alonso, M. D.; Maira, A. J.; Martínez-Arias, A.; Fernández-García, M.; Conesa, J. C.; Soria, J.; Munuera, G. *J. Catal.* **2002**, *212*, 1−9.

10.1021/cm070212w CCC: $37.00
Published on Web 07/19/2007

vapors.[10] Similarly, $Ti_{1-x}Zr_xO_2$ materials with $x < 0.10$ present higher photoactivity than anatase TiO_2 for the degradation of acetone in the gas phase.[11] Besides, nanosized TiO_2-ZrO_2 binary oxides with multiphasic composition also exhibit an increment in the rate for the photocatalytic degradation of different pollutant in both air and aqueous solutions.[12−15] The surface area increase with respect to TiO_2 at a given firing temperature, the inhibition of rutile formation, the higher surface acidity, or the creation of active defects on the TiO_2 surface have been proposed as possible reasons for this improvement in the photocatalytic performance of these materials.[11−15] However, the relative importance of these factors on determining the overall photoactivity is not well-established. In addition, considering the structural complexity of these materials, in which Zr distribution is frequently difficult to determine, the influence of additional parameters on the catalysts performance cannot be discarded. In this respect, it is worth noting that ZrO_2 presents a significant photocatalytic activity,[16] though lower than that of TiO_2, and its presence as a segregated phase in the catalysts of the TiO_2-ZrO_2 system may also contribute to the enhancement of the degradation rate of the pollutants. Furthermore, to the best of our knowledge, it is still not clear whether the formation of Ti−Zr solid solutions or the synthesis of the corresponding binary metal oxides is the best strategy to achieve the highest photoactivity. Therefore, a more thorough investigation of the correlation between structural and surface characteristics of these materials and photoactivity is warranted, because the gained insight may prompt the preparation of improved catalysts.

With this aim, the present work analyzes the influence of Zr doping level on the photoactivity of anatase-type nanoparticles. $Ti_{1-x}Zr_xO_2$ catalysts with $x = 0$, 0.01, 0.03, 0.06, 0.08, and 0.16 were prepared using reverse microemulsions to ensure an elevated homogeneity at structural level.[17] For comparative reasons, an additional sample of ZrO_2 supported on TiO_2, with a 5.2% molar content of Zr, was obtained in a similar way using a two-stage synthesis: first, the TiO_2 was obtained and then this material was incorporated into the microemulsion containing the Zr precursor. The structural and surface characteristics of these samples were determined by N_2 adsorption isotherms, NH_3 adsorption microcalorimetry, X-ray diffraction, and Raman, FTIR, XANES, EXAFS, and UV−vis spectroscopies. In addition, photocatalytic activity for the degradation of methylcyclohexane (MCH) in the gas phase was measured. This pollutant is representative of the volatile organic compounds, involved in ground-level ozone formation in urban environments.[18]

2. Experimental Section

2.1. Photocatalyst Preparation. Different $Ti_{1-x}Zr_xO_2$ catalysts with $x = 0$, 0.01, 0.03, 0.06, 0.08, and 0.16 samples (hereafter named as TZ*x*, where x stand for the Zr content) were prepared by a reverse microemulsion method following a procedure similar to that described elsewhere.[8] For this purpose, a microemulsion was prepared by blending an aqueous solution containing the adequate amount of $ZrO(NO_3)_2$ $6H_2O$ (Aldrich, 99.9%; 50 mL) with n-heptane (Scharlau, 99%; 427 mL), the surfactant Tritón X-100 (Aldrich; 89 mL), and the co-surfactant *n*-hexanol (Aldrich, 98%; 93 mL). Subsequently, the adequate amount of $Ti(OPr^i)_4$ (Aldrich, 97%) dissolved in 2-propanol (Aldrich, 99.5%) was added to the microemulsion, and the mixture was stirred for 24 h in order to achieve the hydrolysis of the alkoxide. In all cases, a significant excess of Zr was incorporated into the microemulsion in order to obtain the final composition as determined by ICP-AES analysis. The obtained precipitate was decanted by centrifugation, rinsed with methanol, dried first at RT, ground in an agate mortar, and dried again at 383 K for 24 h. Finally, the obtained powders were calcined at 773 K for 3 h. Pure TiO_2 and ZrO_2 were prepared in a similar way. An additional sample of 5.2% ZrO_2 supported on TiO_2 (labeled Z/T) was synthesized in a similar way by adding the previously prepared TiO_2 powder to the reverse microemulsion containing the zirconyl nitrate solution.

2.2. Characterization Techniques. The BET surface area was obtained from the N_2 adsorption isotherms measured at 77 K in a Micromeritics 2100 automatic apparatus. Powder XRD patterns of the samples were recorded on a Seifert XRD 3000P diffractometer using nickel-filtered Cu Kα radiation in the Bragg−Brentano geometry. The average particle size was calculated according to the Scherrer equation from the width of the (101) reflections of anatase, whereas unit-cell parameters *a*, *c*, and the unit-cell volume were calculated by a least-squares fitting of the experimental data to the equation for tetragonal symmetry

$$d_{(hkl)}^{-2} = (h^2 + k^2)\, a^{-2} + l^2 c^{-2}$$

where $d_{(hkl)}$ is the distance between the (*hkl*) crystal planes. Microstrain data, calculated by the Williamson-Hall method,[19] were also obtained from the analysis of the XRD profiles.

The microcalorimetric studies of ammonia adsorption were carried out in a differential heat-flow microcalorimeter of the Tian-Calvet type C80 from Setaram, connected to a conventional volumetric apparatus. The adsorption temperature was maintained at 353 K in order to limit physisorption. Each sample was evacuated overnight at 423 K and cooled to the adsorption temperature under vacuum. Then, successive small doses of the probe gas were contacted with the sample. The equilibrium pressure was measured by means of a Baratron pressure transducer MKS Instrument, and the run was stopped at a final equilibrium pressure of 666.6 Pa. The differential heats of adsorption (Q_{diff}) were obtained as the ratio between the exothermic integrated values of each pulse (ΔQ_{int}) and the adsorbed amount (n_a).

A spectroscopic characterization of the samples was also performed. Laser Raman spectra were obtained with a Renishaw Micro-Raman System 1000 equipped with a cooled CCD detector (−73 °C) and a holographic super-Notch filter that removes the

(9) Lin, J.; Yu, J. C.; Lo, D.; Lam, S. K. *J. Catal.* **1999**, *183*, 368−372.
(10) Fresno, F.; Tudela, D.; Coronado, J. M.; Fernández-García, M.; Hungría, A. B.; Soria, J. *Phys. Chem. Chem. Phys.* **2006**, *8*, 2421−2430.
(11) Yu, J. C.; Lin, J.; Kwok, R. W. M. *J. Phys. Chem. B* **1998**, *102*, 5094−5098.
(12) Fu, X.; Clark, L. A.; Yang, Q.; Anderson, M. A. *Environ. Sci. Technol.* **1996**, *30*, 647−653.
(13) Zorn, M. E.; Tompkins, D. T.; Zeltner, W. A.; Anderson, M. A. *Appl. Catal., B* **1999**, *23*, 1−8.
(14) Schattka, J. H.; Shchukin, D. G.; Jia, J. G.; Antonietti, M.; Caruso, R. A. *Chem. Mater.* **2002**, *14*, 5103−5108.
(15) Zhang, Y. H.; Xiong, G. X.; Yao, N.; Yang, W. S.; Fu, X. Z. *Catal. Today* **2001**, *68*, 89−95.
(16) Botta, S. G.; Navío, J. A.; Hidalgo, M. C.; Restrepo, G. M.; Litter, M. I. *J. Photochem. Photobiol., A* **1999**, *129*, 89−99.
(17) Eriksson, S.; Nylen, U.; Rojas, S.; Boutonnet, M. *Appl. Catal., A* **2004**, *265* (2), 207−219.
(18) Rappenglück, B.; Fabian, P. *Atmos. Environ.* **1999**, *33*, 3843−3857.
(19) Zhou, X. D.; Huebner, W. *Appl. Phys. Lett.* **2001**, *79*, 3512.

elastic scattering. The samples were excited with the 514 nm Ar line. The spectral resolution is 3 cm^{-1} and the spectra acquisition consisted of three accumulations of 10 s. DRIFTS spectra of the samples were recorded in a Bruker Equinox 55 FT-IR spectrometer equipped with a MCT detector cooled with liquid N_2 and using a praying mantis device (Harrick). The spectra were recorded in atmospheric air by accumulation of 100 scans with a 4 cm^{-1} resolution. UV−visible diffuse reflectance spectroscopy experiments were performed with a Shimadzu UV2100 apparatus, with $BaSO_4$ as reference. Estimations of the band gap energy for direct and indirect transitions were obtained from the absorption coefficient according to the procedure described elsewhere.[20] XANES and EXAFS experiments at the Ti−K and Zr−K edge were performed on line BM-29 at ESRF (Grenoble, France). A Si (111) double crystal monochromator and a detuning of 30% were used. Experiments were carried out using three N_2/O_2 ionization chambers. The energy scale was simultaneously calibrated by measuring a Ti/Zr film placed before the third ionization chamber.

2.3. Photocatalytic Activity Measurements. The photocatalytic oxidation of methylcyclohexane was tested in a continuous flow annular photoreactor, consisting of two concentric tubes of Pyrex externally illuminated by four symmetrically positioned lamps of black light (Sylvania, 6WBLB-T5, maximum emission at 365 nm) or daylight (Sylvania, F6W/D, UV content of 3%, maximum emission at 435 nm). The gas flowed through the space between the two cylinders at a rate of 100 cm^3 min^{-1}. A concentrated suspension of the catalyst in ethanol was spread on the external surface of the inner glass cylinder in such a way that after drying at RT, the catalyst forms a relatively uniform coating. The amount of catalyst (ca. 0.035−0.040 g) and the illuminated area were approximately the same in all the photocatalytic experiments. Methylcyclohexane (Carlos Erba, 99%) was introduced into the stream of oxygen by means of a syringe pump (Cole Parmer 74900-Series) at the rate appropriate for achieving a concentration of ca. 700 ppmv. Similarly, the water content of the gas was controlled by a second syringe pump, allowing the experiments to be performed either under humid (ca. 75% relative humidity) or dry conditions (<1% RH). Before illumination, the system was equilibrated in the dark for at least 1 h, by flowing the reactive mixture. Analysis of the outlet flow was carried out by means of a Hewlett-Packard G1800 MS-GC, equipped with a HP5 capillary column (0.25 mm I. D. × 30 m) and using the SIM mode of the detector.

3. Results and Discussion

3.1. Textural Properties. The textural data of the samples, obtained from the N_2 adsorption isotherms at 77 K, are summarized in Table 1. It can be observed that the solid solutions with higher content of Zr ($x \geq 0.06$) have larger BET surface area than pure titania. It has been reported that the addition of a second metal such as zirconium increases the specific surface area of the TiO_2-based photocatalysts,[12,21] although in this case, the increase in Zr content leads to only modest changes in the BET surface area. Previous studies claim that this increase is due to the presence of zirconium as ZrO_2, which inhibits crystalline growth of a solid solution,[11] but we have no evidence of the existence of ZrO_2 in our samples (see below). On the contrary, the sample Z/T exhibits the smallest specific surface area.

Table 1. Structural and Textural Data of the Samples

sample	S_{BET} (m^2 g^{-1})	mesopore volume (cm^3 g^{-1})	crystal size[a] (nm)	cell volume[b] (Å^3)	strain[c] ($\Delta d/d$)
TiO_2	52	0.115	12.8	135.7	0.00219
ZrO_2	73	0.139	9.4		
TZ1	57	n.m.[d]	12.6	135.9	0.00226
TZ3	49	0.055	15.4	135.6	0.00162
TZ6	71	n.m.[d]	14.3	135.9	0.00289
TZ8	76	0.053	9.5	137.8	0.00656
TZ16	99	n.m.[d]	10.6	138.2	0.00770
Z/T	34	0.129	13.8	135.9	0.00212

[a] Estimated from XRD data, using the Scherrer equation. [b] Anatase crystallites. [c] Calculated using the Williamson−Hall method. [d] n.m. = not measured.

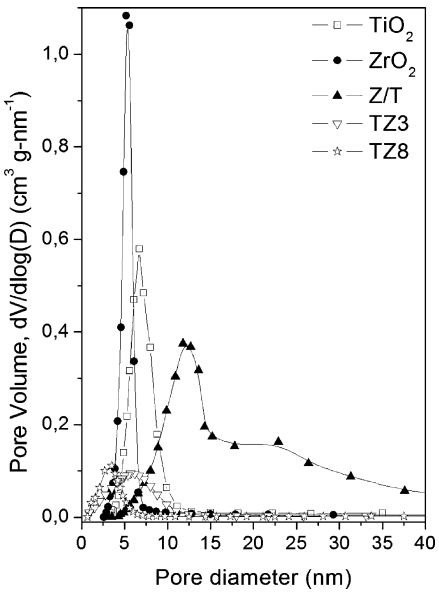

Figure 1. Pore size distribution of some of the catalysts synthesized.

The N_2 adsorption isotherms of all the studied materials are of type IV, as indicated by the hysteresis loop that is associated with the capillary condensation of gases within mesopores.[22] Figure 1 displays the pore size distribution of some of these materials. Pure oxides ZrO_2 and TiO_2 show a very sharp unimodal pore arrangement, whereas mixed oxides present lower porosity with a slightly broader size distribution. Therefore, a direct correlation between surface area and mesopore volume is not found (see Table 1). These results suggest the existence of different forms of particle aggregation among the studied samples. On the other hand, sample Z/T shows a rather wide pore size distribution, with a considerably larger average pore diameter. This fact can be related to the small specific surface of this sample.

3.2. Structural Characterization. The XRD patterns (see Figure 2) indicate that all Ti−Zr samples have an anatase-type structure, with the crystallinity of the materials being slightly lower for the samples with higher Zr content ($x \geq 0.08$). Neither the TiO_2 nor the binary systems contain rutile phase, a polymorph that is considered less photoactive than anatase.[2] Although the thermodynamically stable phase of bulk ZrO_2 below 1200 °C is monoclinic, the ZrO_2 prepared

(20) Serpone, N.; Lawless, D.; Khairutdinov, R. *J. Phys. Chem.* **1995**, *99*, 16646.
(21) Daturi, M.; Cremona, A.; Milella, F.; Buca, G.; Vogna, E. *J. Eur. Ceram. Soc.* **1998**, *18*, 1079.
(22) Rouquerol, F.; Rouquerol, J.; Sing, K. *Adsorption by Powders and Porous Solids: Principles, Methodology and Applications*; Academic Press: London, 1999.

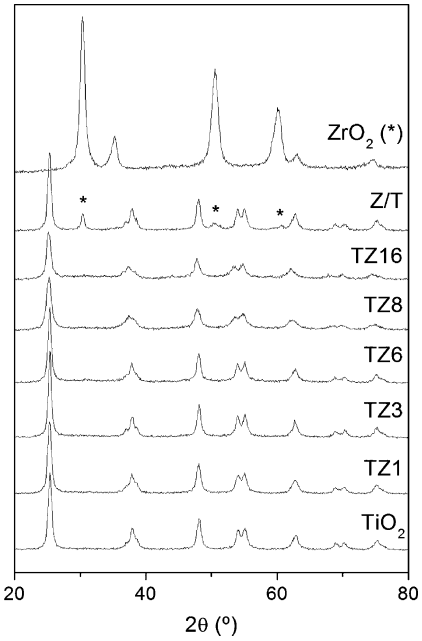

Figure 2. XRD spectra of Ti−Zr mixed oxides and references (pure oxides).

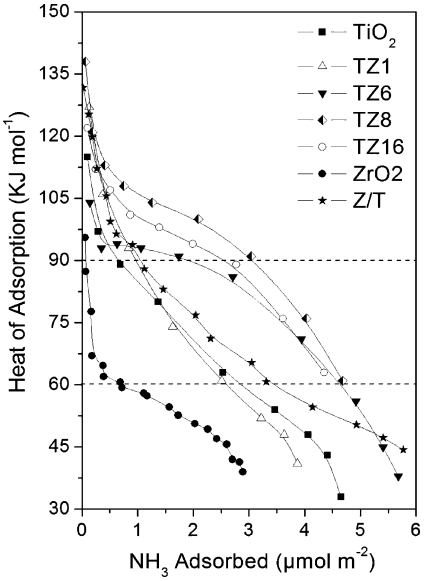

Figure 3. Differential heats for NH_3 adsorption, as a function of the adsorbed amount (μmol m^{-2}).

in this study by the microemulsion method displays the metastable tetragonal phase. The formation of this polymorph is favored by decreasing the size of zirconia particles below ca. 30 nm because of the changes in the surface free energy and strain.[23] Z/T diffraction pattern also shows the presence in this sample of tetragonal ZrO_2, but this phase is not detected in any other Ti−Zr sample.

The particle size ranges from 9.5 to 15.4 nm, with the samples with higher Zr content having lower crystallite sizes. This fact could be associated with the slight increment of surface area observed in these solid solutions. On the other hand, diffraction peaks of anatase shifts to lower diffraction angle in the samples containing Zr, with this displacement being more significant for samples with $x \geq 0.08$. This observation is consistent with Zr incorporation into the TiO_2 lattice, because an increment in the cell volume is expected by the partial substitution of Ti^{4+} by Zr^{4+}, which has a larger ionic radius (0.72 vs 0.60 Å). The Williamson−Hall method has been used to separate the effect of size and the strain in the nanocrystals from the variation of the peak width with 2θ. The strain can be the result of a nonuniform application of stress in the lattice of the nanoparticles and reflects variations in cell dimensions within the sample. Oxygen vacancies and different types of defects can also lead to strain in the lattice of a nanoparticle.[23] Similarly to other changes observed in the X-ray diffraction parameters, the strain experiences a considerable increase in samples with Zr content higher than 6% (see Table 1). All these data suggest that an incipient structural transformation of the anatase structure start to take place in the $Ti_{1-x}Zr_xO_2$ materials with $x > 0.06$.

3.3. Surface Acidity. Figure 3 shows the differential heats for NH_3 adsorption, as a function of the adsorbed amount (μmol m^{-2}), for some of the samples under study outgassed at 423 K. TiO_2 displays a heterogeneous distribution of acid sites with heats of adsorption decreasing constantly from 120 kJ mol^{-1} as the coverage increases, implying a surface made up of several kinds of sites. On the other hand, ZrO_2 sample showed the lowest initial heat of adsorption (ca. 100 kJ mol^{-1}), leading to lower values than those for TiO_2 for all coverages. The sharp decrease in Q_{diff} observed at low coverages indicates the presence of a small concentration of strong Lewis type acid sites. For higher coverages, the rate of fall is lower, and this fact can be ascribed to a more homogeneous distribution of sites of both Lewis and Brønsted type for ZrO_2. Its profile reflects that the majority of these sites are weak with heats of adsorption of less than 60 kJ mol^{-1}.

The shape of the calorimetric curve observed for sample Z/T is very similar to that observed for pure titania. However, the initial heats of adsorption are higher, ca. 140 kJ mol^{-1}, and the Q_{diff} profile for Z/T lies above that for TiO_2 in the whole range of coverages. TZ1 exhibits the same behavior than TiO_2, whereas samples TZ6, TZ8, and TZ16 are more acidic in terms of concentration and strength of sites than the parent oxides. The initial heats of adsorption, about 120 and 140 kJ mol^{-1} for TZ6 and TZ8, respectively, are higher than the one obtained for TiO_2, as in the case of Z/T. The curves of the TZ samples can be divided in three regions: an initial part at coverages lower than 0.7 μmol m^{-2}, where the heats of adsorption decrease sharply; a second region at coverages between 0.7 and 3 μmol m^{-2}, where the heats slowly fall, indicating a set of more homogeneous sites; and the last region, until physisorption is reached, where the rate of fall is again higher. The profile for TZ6, where the amount of Zr is lower, is beneath that for TZ8 and TZ16 in all the range of coverages. The acid strength of all the samples can be compared on the basis of the calculated fraction of sites which give rise to $Q_{diff} \geq 90$ kJ mol^{-1} over the total sites (measured at an equilibrium pressure of 1 Torr), n_{90}/n_T, which gives an idea of the number of strong acid sites. Taking this parameter into account (Table 2), the observed trend is $ZrO_2 < TiO_2 <$ Z/T < TZ1 < TZ6 < TZ16 < TZ8. This indicates

(23) Fernández-García, M.; Martínez-Arias, A.; Hanson, J. C.; Rodriguez, J. A. *Chem. Rev.* **2004**, *104*, 4063.

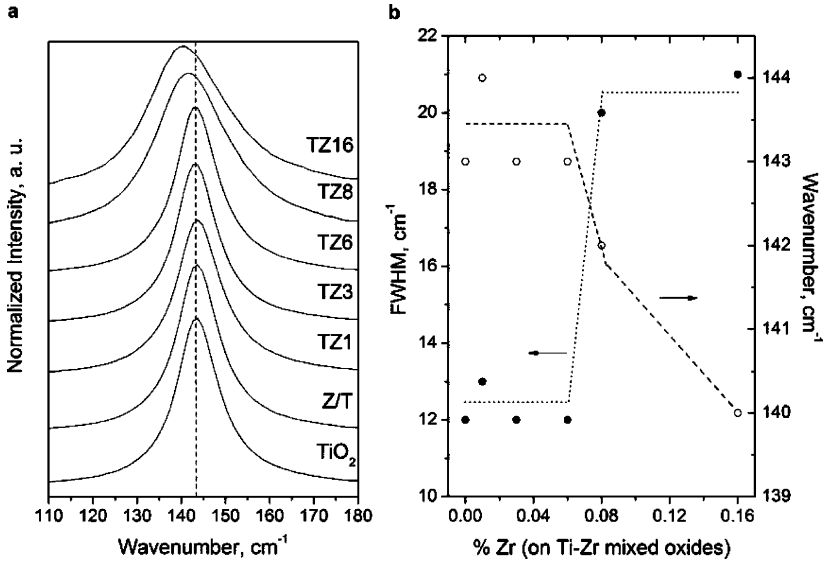

Figure 4. (a) Detail of Raman spectra, corresponding to the first E_g mode; (b) fwhm and peak position of the E_g Raman mode of the anatase-type structure present in the Ti−Zr samples. Closed symbols, fwhm; open symbols, energy position; dashed lines are used only as a reference guide.

Table 2. Surface Acidity of Ti−Zr Samples and Pure Oxides

sample	total acidity, n_T (μmol m^{-2})	acidity $Q_{diff} > 90$ kJ mol^{-1}, n_{90} (μmol m^{-2})	n_{90}/n_T ratio
TiO_2	3.24	0.67	0.21
ZrO_2	1.65	0.07	0.04
TZ1	2.69	0.98	0.36
TZ6	4.87	1.92	0.39
TZ8	4.30	3.07	0.71
TZ16	4.28	2.57	0.60
Z/T	4.07	1.05	0.26

the influence of Zr in surface acidity of titania, because there is a significant increase of n_{90}/n_T in all the solid solutions synthesized. The addition of Zr results in a modification of the energy distribution and strength of surface adsorption sites. The increment of surface acidity in mixed oxides has been generally attributed to a charge imbalance, associated with heterometallic bonding formation. In this particular case, the generation of Ti−O−Zr bonds requires the formation of additional surface hydroxyls groups coordinated to Zr, which can act as strong acid sites.[12,24,25] This is consistent with the fact that Z/T and TZ6, having approximately the same molar content of Zr, show significant different profiles. A limit in the increase of acidity is also observed, with the TZ8 sample having the highest surface acidity, probably because of changes in the Zr coordination spheres in TZ16, which progressively resemble those of ZrO_2.

The ammonia adsorption calorimetric data were supported by DRIFTS analysis of the catalysts surfaces after the ammonia adsorption. It is worth emphasizing the presence of a band at ca. 1443 cm^{-1} in the spectra of the different solid solutions (very weak in TZ1) corresponding to the asymmetric bending mode of NH_4^+ ion, which suggests the protonation of NH_3 chemically adsorbed and the presence of Brønsted acid sites on the Ti−Zr solid solutions surfaces.[26,27]

3.4. Spectroscopic Characterization. Consistent with XRD data, Raman spectroscopy also provides evidence that all Ti−Zr samples present anatase-type structures, with the crystallinity of the material being lower with increasing Zr content. The bands observed at about 143, 197, 397, 516, and 639 cm^{-1} can be assigned to, respectively, the six fundamental vibrational modes of anatase E_g, E_g, B_{1g}, $A_{1g}+B_{1g}$, and E_g. No significant changes with respect to undoped TiO_2 are observed in either samples with $x < 0.08$ nor in the ZrO_2/TiO_2 material, whereas a red shift and a broadening of the most intense E_g peak takes place in samples with $x \geq 0.08$, as can be clearly observed in Figure 4a. Analysis of the FWHM and energy position of the first E_g Raman mode as a function of the Zr at % show the presence of a breaking point for Zr content around 8 at % (Figure 4b). As mentioned before, these samples have a smaller crystallite size, which would lead to a broadening of the 143 cm^{-1} band according to the phonon confinement model.[28] Taking into account exclusively the phonon confinement effect, a blue shift would be expected with decreasing the particle size.[29,30] On the contrary, in the Raman spectra of these Ti−Zr samples, a shift to lower wavenumber is observed. This displacement can be related to the lattice expansion observed in materials with higher Zr content and smaller particle size. It is known that variations in the pressure, temperature, or composition of the samples lead to changes in the unit-cell volume that can produce a shift in the energy position of Raman modes. An estimation of this shift can be determined by the so-called Grüneisen parameter, γ.[31] The Grüneisen parameter for a certain vibrational mode, γ_i, is defined by the following equation

$$\gamma_i = -(d \ln \omega_i / d \ln V) \quad (1)$$

where ω_i is the frequency of the vibrational mode (wave-

(24) Liu, Z.; Tabora, J.; Davis, R. J. *J. Catal.* **1994**, *149*, 117.
(25) Mao, D. S.; Li, G. Z.; Chen, Q. L. *Chin. J. Catal.* **2004**, *25*, 501.
(26) Hermann, M.; Boehm, H. P. Z. *Anorg. Allg. Chem.* **1969**, *368*, 73.
(27) Hadjiivanov, K. *Appl. Surf. Sci.* **1998**, *135*, 331.
(28) Kelly, S.; Pollak, F. H.; Tomkiewicz, M. *J. Phys. Chem. B* **1997**, *101*, 2730.
(29) Bersani, D.; Lottici, P. P.; Ding, X. Z. *Appl. Phys. Lett.* **1998**, *72*, 73.
(30) Iida, Y.; Furukawa, M.; Aoki, T.; Sakai, T. *Appl. Spectrosc.* **1998**, *52*, 673.
(31) Hirata, T. *Phys. Status Solidi* **1998**, *209*, 17.

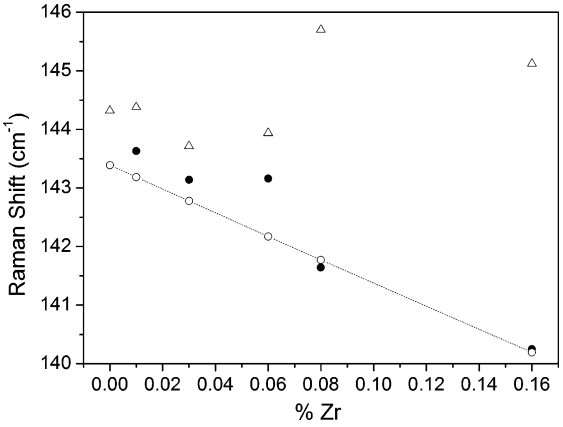

Figure 5. Open circles and dashed lines represent the theoretical Raman Shift expected from volume cell increment, taking into account the Grüneisen parameter; open triangles represent the theoretical Raman shift expected from phonon confinement; black circles represent the experimental data.

number, in cm^{-1}) and V is the cell volume. The possible change in cell volume caused by modifications in the chemical composition is given by the expression $V = V_0 + \theta x$, where x corresponds to the amount of solute metal in a substitutional solid solution ($Ti_{1-x}Zr_xO_2$) and V_0 is the unit-cell volume at $x = 0$. Parameter θ, representing the derivative of V with respect to x, can be either positive or negative depending on the effect of x variation on the cell volume (expansion or contraction). In this case and assuming that γ_i is x independent, γ_i can be approximated by γ_0, which is the Grüneisen parameter at $x = 0$. Besides, considering that θ is constant and equal to $\Delta V/\Delta x$, the following expression can be derived

$$\ln\frac{\omega_i}{\omega_0} = \gamma_0 \ln\left(1 + \frac{\theta x}{V_0}\right) \qquad (2)$$

where ω_0 is the frequency for the vibrational mode at $x = 0$. The value of γ_0 used in the calculations, 0.83, is based on the results obtained by T. Hirata[31] for samples $Ti_{1-x}Zr_xO_2$. Figure 5 shows that the theoretical Raman Shift expected from volume cell increment, taking into account the Grüneisen parameter, reasonably suits the changes observed in our samples, suggesting that no other effect seems to dominate the band broadening.

Table 3. Energy Position and fwhm of the First E_g Raman Mode and Band Gap Estimations (obtained from the UV−vis spectra) of the Samples Synthesized

			band gap estimations (eV)	
sample	Raman shift	Raman fwhm	direct	indirect
TiO_2	143	12	3.2	2.9
ZrO_2			3.9	3.1
TZ1	144	13	3.2	2.9
TZ3	143	12	3.2	2.8
TZ6	143	12	3.2	2.8
TZ8	142	20	3.2	2.9
TZ16	140	21	3.2	2.9
Z/T	143	12	3.2	3.0

Quantitative estimations of the band gap energy for direct and indirect transitions can be obtained from the UV−vis DRS spectra (Table 3) and show the absence of significant changes in E_{bg} with Zr incorporation in the TiO_2 lattice.

Ti K edge XANES spectra of these samples (Figure 6a) show three peaks in the preedge region, namely, A_1, A_3, and B, corresponding to slightly distorted octahedrally coordinated titanium atoms. These peaks appear at the same energy as in the anatase reference material and no significant differences are detected in the spectra, suggesting a similar local symmetry in all of them. In the TZ16 sample, an additional peak can be observed as a weak shoulder on the low-energy side of A_3, namely A_2, associated with the presence of five-coordinated Ti species on the surface of the anatase particles, whose contribution increase as the particle size decreases.[32,33] On the other hand, a bigger distortion of the Ti octahedron in this catalyst, generated by the Zr inclusion into the TiO_2 structure, could also be modifying the preedge structure.[34]

Spectra at the Zr K edge of these materials were also recorded (Figure 6b). The edge and/or preedge intensity and width are parameters to be considered, because they provide information about the absorber symmetry, and it is commonly defined as the full width at half-maximum of the main peak

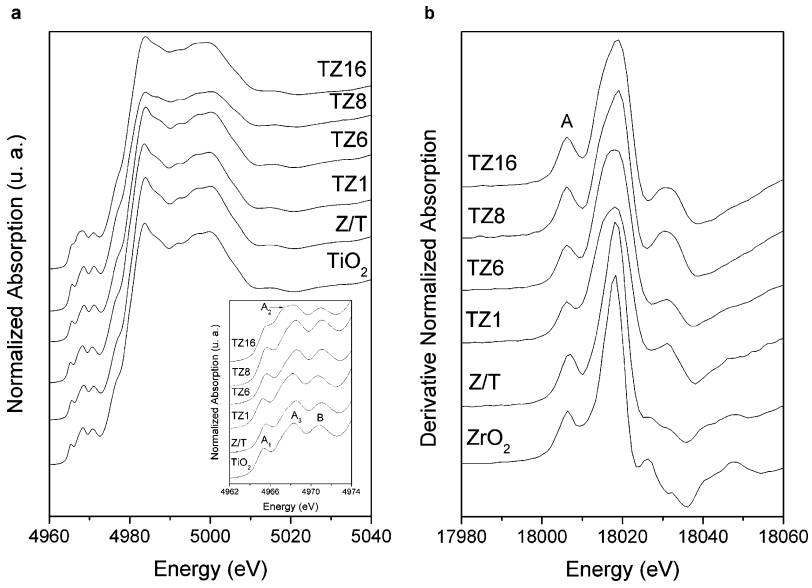

Figure 6. (a) XANES spectra of Ti K edge. Inset shows detail of the preedge region; (b) first derivative of Zr K edge XANES spectra.

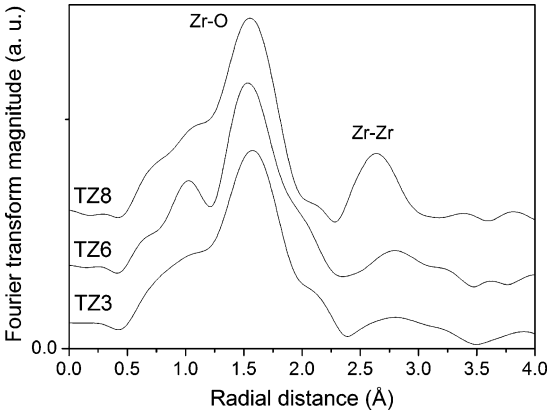

Figure 7. Fourier transforms of Zr K edge EXAFS spectra of TZ3, TZ6, and TZ8 solid solutions.

in the first derivative. The peak, namely, A, is observed in the preedge region of the XANES spectra and corresponds to the 1s → 4d transition, forbidden in the absence of a d−p orbital mixing. Considering that noncentrosymmetric geometries allow this mixing and that the intensity of this peak is lower for TZ1 and similar to that of zirconia for TZ16, it can be concluded that Zr−O coordination is more symmetric (centrosymmetric type) in TZ1 than in TZ16 (noncentrosymmetric type), which resembles more that of ZrO_2. Figure 7 displays the Fourier transforms of Zr K edge EXAFS spectra of some of the samples synthesized. The peak at ca. 1.5 Å corresponds to the first Zr−O coordination shell, and no significant differences in intensity are observed between the different materials tested. On the other hand, a considerable increase in intensity is detected for TZ8 in the peak at ca. 2.75 Å. XAS study at Zr K edge suggests a random distribution of Zi^{4+} ions in the host oxide in solid solutions with $x < 0.06$ (Zr in an octahedral symmetry). The absence of neighbors at cation−cation coordination shell suggests an important local distortion in the structure. For Zr molar contents above 6%, Zr^{4+} ions progressively depart from octahedral positions, with a local symmetry similar to that of tetragonal ZrO_2, and then second neighbors with Zr nature appear. The fitting analysis of the results unequivocally show the presence of both Zr and Ti ions at the second coordination shell. However, the presence of two scatters together with the significant inhomogeneity of the Zr−O first shell (see the corresponding broad peak at $R < 2$ Å in Figure 7) limit the accuracy of numerical results (not reported here).

Summarizing, it can be concluded that Raman and XAS spectroscopies show, in agreement with XRD results, that despite the fact that the anatase structure is retained by the samples with Zr content higher than 6%, local order modifications are found above this limit. These transformations include the shift of the most intense E_g Raman band due to the unit-cell expansion, and the changes in the coordination spheres of Ti and, particularly, Zr. On the other hand, in the sample Z/T, the two phases are basically unaffected and keep the characteristics of the pure oxides. In contrast, the electronic characteristics of the Zr-doped materials are very similar to those of pure anatase TiO_2, according to their UV−vis spectra.

3.5. Photocatalytic Tests. The photocatalytic activity of the samples was tested for the photooxidation of MCH in air under UV illumination, using both humid (ca. 75% relative humidity) and dry (<1% RH) air streams. Under these conditions, the only products detected in the gas phase were CO_2 and H_2O. The reference photocatalyst TiO_2 Degussa P25 was also assayed for comparative reasons.

Figure 8a shows the progress of MCH conversion with irradiation time in a humid oxygen stream for different photocatalysts. As can be seen, TiO_2 Degussa P25 shows a significant deactivation under humid conditions. In contrast, our catalysts present a conversion that progressively increases to reach a steady state after about a 40−50 min period. Table 4 displays the steady-state MCH conversion of the different photocatalysts tested. Data show that, at high relative humidity, there is a clear enhancement in photoactivity for all the $Ti_{1-x}Zr_xO_2$ samples with respect to TiO_2, whereas ZrO_2/TiO_2 exhibits a slightly lower conversion. An increase in the % Zr molar content leads, initially, to an increase in MCH conversion although a significant decrease is observed in TZ16 sample. ZrO_2, used as a reference material, did not

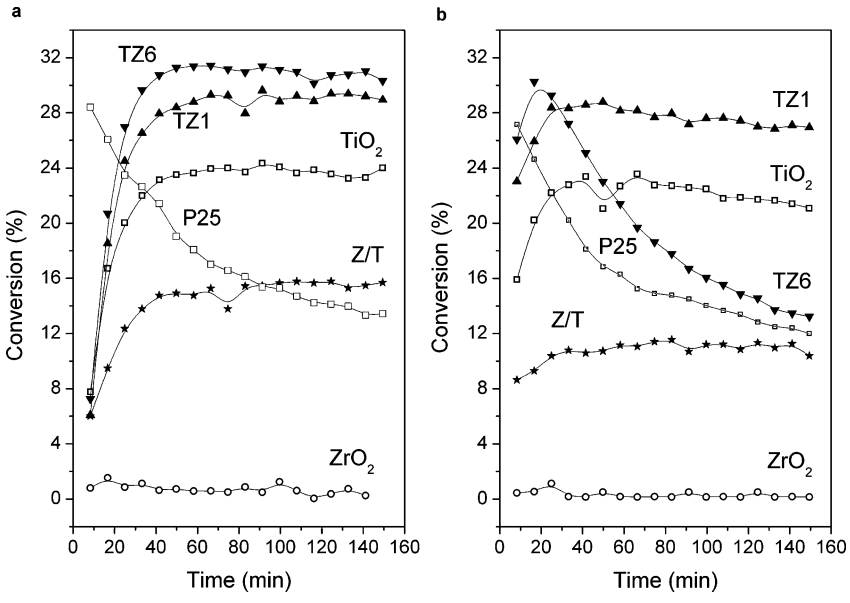

Figure 8. MCH conversion progress with irradiation time: (a) under humid conditions and (b) under dry conditions.

Table 4. Steady-State MCH Conversion Data for the Ti−Zr Samples and References

	steady-state conversion (%)	
sample	UV, HR ≈ 75%	UV, HR < 1%
P25	14[a]	13[a]
TiO_2	23.8	21.5
TZ1	29.0	27.1
TZ3	31.4	10.1
TZ6	30.9	13.8[a]
TZ8	33.3	20.4
TZ16	23.8	16.6
Z/T	15.3	11.0
ZrO_2	0.7	0.1

[a] The values correspond to the conversion after 140 min of illumination.

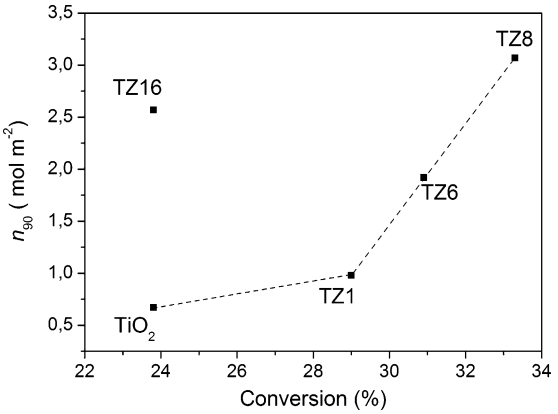

Figure 9. Relation between MCH conversion under humid conditions and surface acidity, measured as n_{90}.

exhibit any photocatalytic activity, as expected considering its high band gap energy, which does not match the emission spectrum of the light source utilized. The same relative rank of photoactivity was obtained for these samples when daylight lamps were used instead of the UV ones, but the conversions measured in these conditions showed a 5-fold decrease. These data perfectly correlate with the ratio between the UVA irradiance of the two light sources and consequently discard any contribution of the visible light to the reaction, as expected considering the optical spectra of these materials. Apparent photonic efficiencies for MCH removal varied between 2 and 7% depending on the photocatalyts.

As described above, the incorporation of Zr into the anatase structure does not lead to significant changes in the electronic properties of samples with $x < 0.08$. Consequently, the improved performance of the solid solutions can be related, basically, to the modifications of the surface characteristics of these materials. First of all, the increase in specific area with the incorporation of Zr has to be considered, as it favors the adsorption of the reactants on the catalyst surface. However, because the sample with highest specific area did not exhibit the best performance and Zr incorporation decreases the porosity, it follows that other contributions must be taken into account. In this case, the photocatalytic activity for the oxidation of MCH under humid conditions seems to be related to the surface acidity of these materials. As shown in Figure 9, an increase in MCH conversion occurs as the number of strong acid sites rises. As mentioned before, the higher acidity in these catalysts would be caused by the formation of strongly acidic surface hydroxyls These surface groups could accept the photogenerated holes, avoiding recombination and taking part in the oxidation of the organic molecules adsorbed on the surface, as has been reported previously.[35,36] The beneficial effect of surface acidity is, however, counteracted in solid solutions with $x \geq 0.08$ because of the structural changes detected by XAS analysis, which imply modifications in Zr coordination shells that probably set a limit in the increase of acidity for TZ16. These modifications may lead to an increment in the number of recombination centers, and consequently, they reduce the efficiency of the photocatalytic process.

However, though the photocatalytic activity increases with increasing Zr content under humid conditions and reaches a maximum for TZ8, under dry conditions (Figure 8b), the activity of the $Ti_{1-x}Zr_xO_2$ samples with $x > 0.01$ is markedly lower, especially after prolonged irradiation. This activity decrease is due to a significant deactivation of the most active photocatalytic sites. In all cases, the reaction rate is lower than under humid conditions. Similar results have been previously obtained for the photocatalytic removal of MCH using $Ti_{1-x}Sn_xO_2$.[37] Furthermore, although Degussa P25 and solid solutions with $x > 0.01$ experience a pronounced deactivation, conversion remains practically constant for TiO_2, Z/T, and TZ1. It is worth noticing that TZ3, TZ6, and TZ8 photocatalysts, with the best performance at HR ≈ 75%, suffer the most marked deactivation. This behavior is very likely due to the presence of intermediate products adsorbed on the surface, not detected in the gas effluents, and associated with an intense orange color of the materials used at HR < 1%. The absence of water vapor in the oxygen stream favors the adsorption of byproducts and hinders surface hydroxyls regeneration, leading to photocatalyst deactivation. On one hand, microcalorimetric results suggest that the increase in the number and strength of acid sites is responsible for the improvement in the solid solutions observed in the photocatalytic activity at HR ≈ 75% in comparison to pure TiO_2, although in the other hand, the higher accumulation of organic molecules generated in the reaction at HR < 1% would lead to their fast deactivation. The presence of fewer strong acid sites (n_{90}) is observed in materials that exhibit no significant deactivation. In this way, TZ1 has, among all materials modified by Zr incorporation, the appropriate balance of factors enhancing the photoactivity.

Figure 10 shows a detail of the DRIFT spectrum of sample $Ti_{0.94}Zr_{0.06}O_2$, used in the photocatalytic oxidation of MCH. This sample experiences one of the most marked deactivation observed under dry conditions, in spite of being one of the most active ones at 75% RH. Because the contribution of the bulk sample has been removed by subtraction of the spectrum of the fresh material, the bands appearing in the spectrum at 1715, 1690, 1544, 1410, and 1317 cm^{-1}

(32) Luca, V.; Djajanti, S.; Howe, R. F. *J. Phys. Chem. B* **1998**, *102*, 10650.
(33) Choi, H. C.; Jung, Y. M.; Kim, S. B. *Vib. Spectrosc.* **2005**, *37*, 33.
(34) Salama, T. M.; Tanaka, T.; Yamaguchi, T.; Tanabe, K. *Surf. Sci. Lett.* **1990**, *227*, L100.
(35) Do, Y. R.; Lee, W.; Dwight, K.; Wold, A. *J. Solid State Chem.* **1994**, *108*, 198.
(36) Papp, J.; Soled, S.; Dwight, K.; Wold, A. *Chem. Mater.* **1994**, *6*, 496.
(37) Fresno, F.; Coronado, J. M.; Tudela, D.; Soria, J. *Appl. Catal., B* **2005**, *55*, 159.

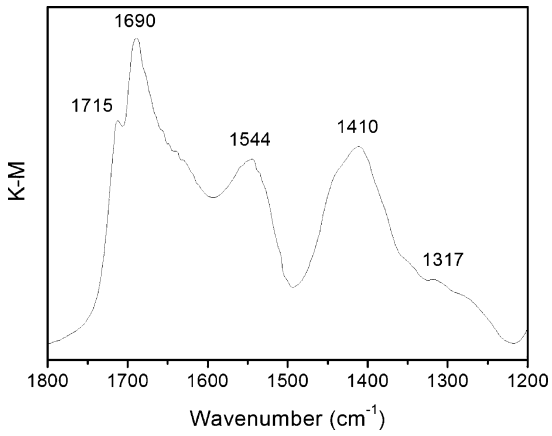

Figure 10. Detail of the DRIFT spectrum of TZ6 photocatalyst, after being used for the photocatalytic oxidation of MCH under dry conditions.

correspond exclusively to species adsorbed during the reaction. Although partially oxidized products have not been detected in the gas stream, the presence of these peaks in the spectrum indicates the accumulation of organic molecules on the surface of the catalyst during the photocatalytic reaction. The peaks at 1715 and 1690 cm^{-1} can be associated with the γ (C═O) mode of different carbonyl compounds, whereas bands at 1544 and 1410 cm^{-1} can be ascribed to the stretching modes of carboxylate species (acetate or formate).[38] The band at 1410 cm^{-1}, along with the one appearing at 1317 cm^{-1}, could also correspond to the bending mode of CH_2^- and CH_3^- groups. The adsorption of organic molecules on the catalyst during the oxidation of MCH is parallel to the dehydratation of the surface, as evidenced by the loss of intensity of the band centered at about 3400 cm^{-1} (result not shown). In the absence of water vapor, the presence of these byproducts along with the surface dehydroxilation can be related to the progressive deactivation of the samples. Similar observations have been made for other photocatalytic systems.[38−40]

(38) Coronado, J. M.; Kataoka, S.; Tejedor-Tejedor, I.; Anderson, M. A. *J. Catal.* **2003**, *219*, 219.
(39) Maira, A. J.; Yeung, K. L.; Soria, J.; Coronado, J. M.; Belver, C.; Lee, C. Y.; Augugliaro, V. *Appl. Catal., B* **2001**, *29*, 327.
(40) Coronado, J. M.; Zorn, M. E.; Tejedor-Tejedor, I.; Anderson, M. A. *Appl. Catal., B* **2003**, *43*, 329.

4. Conclusions

The results obtained in this work indicate that reverse microemulsion synthesis is an adequate method for preparing homogeneous and nanocrystalline Ti−Zr solid solutions. Structural and spectroscopic characterization results reveal that the anatase-type structure is maintained throughout the Ti−Zr series but that significant differences in the local order are found for samples above/below 6 Zr at % content. XANES and EXAFS data indicate that, at low molar contents, Zr randomly substitutes Ti atoms in the anatase lattice. For solid solutions with $x > 0.06$, some modifications are detected in Ti and Zr coordination spheres with the presence of medium-range order; the probability of finding a Zr cation in the Zr second shell remarkably increases with respect to the random situation. In addition, the blue-shift of the most intense E_g Raman resonance can be correlated to the expansion of the cell volume observed for the materials with $x > 0.06$. In contrast, the interband transitions of these semiconductors are not appreciably affected by Zr incorporation.

All $Ti_{1-x}Zr_xO_2$ samples show a significant improvement in the photocatalytic activity at high relative humidity with respect to TiO_2 and ZrO_2/TiO_2 materials. However, in the photocatalytic oxidation of methylcyclohexane under UV illumination and 75% RH, the increase in photocatalytic activity with Zr content reaches a maximum at $x = 0.06$. On the other hand, solid solutions with $x > 0.01$ exhibit a strong deactivation under dry conditions, whereas conversion for TZ1, Z/T, and pure titania remains nearly constant. The number of strong acid sites on the catalyst surface seems to be the main factor responsible of this behavior, although structural effects related to Zr local coordination have an additional influence in solid solutions with $x \geq 0.08$. At HR < 1%, the accumulation of byproducts in the reaction on the catalyst surface would be the reason for the marked deactivation of most acid mixed oxide samples.

Acknowledgment. This study was partially financed by the CICYT projects CTQ2004-03409/BQU and CTQ2004-08232-C02-01/PPQ. The ESR staff is also thanked for the help during XAS experiments. M.D.H.-A. wants to thank the "Comunidad Autónoma de Madrid" (CAM) for the award of her doctoral grant and B.B.-B. thanks the financial support from the ''Ramón y Cajal" program of the Spanish Ministry of Education and Science.

CM070212W